Appl Phys B (2009) 95: 739–744
DOI 10.1007/s00340-008-3332-8

Applied Physics B
Lasers and Optics

Dependence of terahertz radiation on gap sizes of biased multi-energy arsenic-ion-implanted and semi-insulating GaAs antennas

T.-A. Liu · R.-H. Chou · C.-L. Pan

Received: 30 October 2008 / Published online: 11 December 2008

Abstract We investigate the characteristics of terahertz radiation pulses using biased multi-energy arsenic-ion-implanted and semi-insulating GaAs photoconductive antennas with different gap sizes in terahertz time-domain spectroscopy. At a specific fluence excitation, with increasing antenna gap size, the absolute values of the (peak) normalized terahertz waveform minimum (valley), as well as the bandwidth, reveal an increasing trend for multi-energy arsenic-ion-implanted GaAs antennas and a decreasing trend for semi-insulating GaAs antennas. We find that the largest reachable bias fields applied to arsenic-ion-implanted GaAs antennas are higher than those applied to semi-insulating GaAs antennas. On the basis of pump fluence dependences of peak terahertz amplitude, we deduce that multi-energy arsenic-ion-implanted GaAs antennas have the ability to acquire higher THz power at even higher pump fluence in comparison with semi-insulating GaAs antennas.

PACS 85.60.Bt · 85.60.Gz · 73.50.Pz · 61.72.Uj · 85.30.-z · 77.22.Jp · 78.47.Cd · 07.57.Hm

T.-A. Liu (✉)
Center for Measurement Standards, Industrial Technology Research Institute, 321, Sec. 2, Kuang Fu Road, Hsinchu 300, Taiwan
e-mail: liutzean@itri.org.tw

R.-H. Chou · C.-L. Pan
Institute of Electro-Optical Engineering, National Chiao Tung University, 1001 Ta Hsueh Road, Hsinchu 300, Taiwan

R.-H. Chou
e-mail: ronehwa@hotmail.com

C.-L. Pan
e-mail: clpan@faculty.nctu.edu.tw

1 Introduction

Terahertz (THz) radiation pulses from biased photoconductive (PC) antennas have been widely used in various disciplines including chemical, biological, imaging, and telecommunications [1–4]. The emission characteristics of THz radiation are associated with the pump conditions or device structures that we adopt. Hence, the aim of most researchers is to discover an optimum operation for efficient THz radiation generation.

Under fixed pump conditions, the PC antenna factors involving geometries, gap sizes G, and photoconductive materials, will significantly affect the THz emission features of radiation power, peak width, and spectrum. In terms of G, PC antennas with a G larger than 5 mm are able to provide giant THz radiation power [5]. In practical employment, however, such larger-aperture antennas require heavy equipment leading to a confined movement range for the antennas. To overcome this disadvantage, one can utilize mid-aperture antennas with a G ranging from 0.1 to 1 mm, since it provides impetus to generate THz radiation in a compact environment.

Another antenna factor that determines the emission performance of an antenna is its PC materials. From the point of view of electrical properties, PC material with high resistivity is preferred as a substrate, since it can have a large bias applied to it and thus obtain high THz power. To reach this goal, liquid-encapsulated Czochralski-grown or low temperature molecular-beam-epitaxy grown materials have been used during the production of GaAs-based antennas. The former and latter materials are known as semi-insulating GaAs (SI-GaAs) [6] and LT-GaAs. In the optical pump–probe differential reflection measurement, the carrier lifetime of a SI-GaAs based antenna usually has the value of over several picoseconds, while a LT-GaAs based antenna

possesses a carrier lifetime shorter than one picosecond [7], so it can provide a broader emission spectrum than a SI-GaAs antenna [8]. Nevertheless, the drawback of a LT-GaAs antenna is that it is difficult to be reproduced even under the same experimental conditions, except for a specific approach [9]. On the other hand, multi-energy arsenic-ion implantation in GaAs (multi-GaAs:As^+) will result in a highly nonstoichiometric disturbance and lead to material characteristics similar to LT-GaAs. During the fabrication of a multi-GaAs:As^+ antenna, the ion dose can be precisely controlled, implying that such a device has the reproducible property [10]. Moreover, a multi-GaAs:As^+ antenna has a high breakdown voltage and a good carrier mobility, and therefore has replaced the LT-GaAs antenna as a promising candidate for a THz radiation source [11–13].

If the antenna factors are fixed at specific conditions, the variations of pump fluence F and nominal bias field E_b applied to the antennas will have a profound influence on THz emission features as well. Experimentally, one usually observes from pump fluence dependence that the peak THz amplitude grows first at low fluence, while it saturates at a high F [14, 15]. From bias-field dependence, one can observe that the peak THz amplitude, from a large-aperture antenna, scales linearly with the bias field [16]. Theoretically, both types of dependences can be simply described by the scaling rule [17]. Besides the influence of pump fluence and bias field, Ralph and Grischkowsky found that the THz field magnitude will be strongly enhanced if the illumination position of the laser spot approaches the anode of a 80-μm-gap SI-GaAs antenna [18]. This enhanced THz radiation, obtained by asymmetrical illumination, results from the extremely large bias field near the anode, due to material defects.

In the present contribution we report on the characteristics of THz radiation pulses from multi-GaAs:As^+ antennas with varying G, and analyze several essential emission characteristics including the absolute value of the THz waveform minimum (valley), bandwidth, bias field, and pump fluence dependence of peak THz amplitude. The performances of multi-GaAs:As^+ antennas are compared to those obtained from similar devices made of SI-GaAs.

2 Experiments

Our experiments were carried out by employing THz time-domain spectroscopy. We made use of two types of materials to construct THz radiation emitters. One type was fabricated on multi-GaAs:As^+, and the other type was fabricated on highly resistive SI-GaAs. For each type of antenna, we chose five samples with gap sizes G of 0.02, 0.1, 0.2, 0.5, and 1 mm. The antenna consisted of two coplanar strip lines with Au metallic coating layers of 300 nm as illustrated in Fig. 1. The carrier lifetimes for both materials were obtained from the optical pump-probe differential reflection measurement.

The experimental setup for the generation and measurement of THz radiation was similar to the common free-space electro-optical (EO) detection from the emitter of biased PC antennas [19]. The pump or probe pulses, with an 800-nm wavelength and 130-fs pulse width, were also provided by the mode-locked Ti:sapphire laser, operating at the repetition rate of 85 MHz and with the pump power of 500 mW. The laser excitation positions are depicted in Fig. 1. The pump spot size incident on the sample was fixed to approximately 0.1-mm diameter. In the cases of $G = 0.02$ and 0.1 mm, the spot positions were central, with respect to the gap, so that both illuminations were nearly uniform. In the cases of $G = 0.2$, 0.5, and 1 mm, the position of the laser spot was located near the anode in order to obtain an optimum THz radiation. The generated THz radiation beam was thus collimated and focused onto the EO sensor of ZnTe with a thickness of 1.5 mm, by a pair of off-axis paraboloidal mirrors. Since the THz radiation was collected by parabolic mirrors in this experiment, the temporal resolution was limited by group-velocity mismatch between the optical probe beam and THz radiation. The other coherent polarized probe beam was collimated onto the EO crystal and the polarization was modified because of the modified refractive index from the THz field. The probe beam was then transmitted through the analyzer and we sampled the THz field from the time delay between the pump and probe beams.

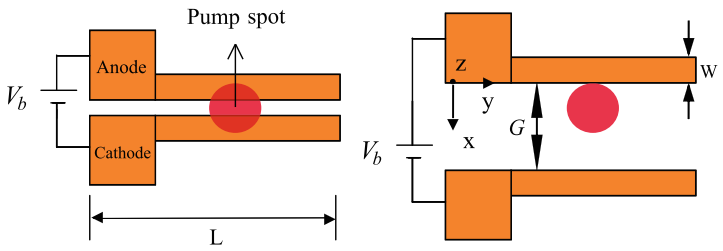

Fig. 1 Schematic representation of DC-biased PC antennas excited by femtosecond laser pulses. L and W are equal to 10 mm and 0.1 mm, respectively. The illuminated regions are indicated by *red circular spots*. The *left-* and *right-hand diagrams* illustrate the uniform illumination for gap spacing $G = 0.02$ or 0.1 mm, and the asymmetric illumination for $G = 0.2$, 0.5, or 1 mm, respectively

3 Results and discussion

3.1 Waveforms and spectra

Figure 2 shows the normalized photoreflectance changes $\Delta R/R$ of multi-GaAs:As$^+$ and SI-GaAs based antennas as a function of the time delay t. Fitting these data to exponential decays yields the results that the carrier lifetimes of the multi-GaAs:As$^+$ and SI-GaAs antennas are 0.8 and 2.5 ps, respectively. Obviously, the carrier lifetime of each antenna is much longer than the pump pulse duration (=0.05 ps).

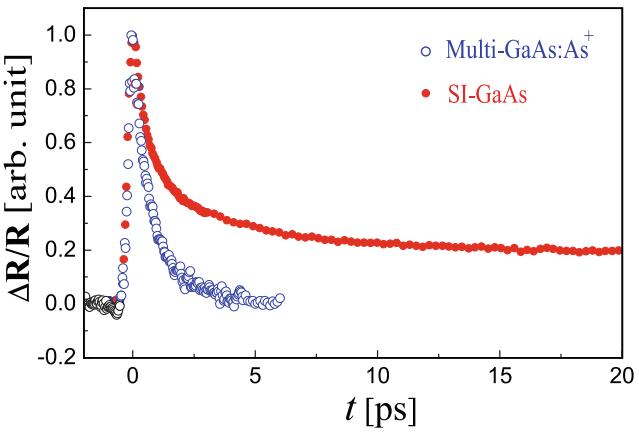

Fig. 2 Transient photoreflectance changes $\Delta R/R$ for multi-GaAs:As$^+$ (*open blue circles*) and SI-GaAs (*solid red circles*)

Figure 3 shows the normalized THz radiation waveforms E_r and their respective Fourier-transformed amplitude $\tilde{E}_r$ spectra from multi-GaAs:As$^+$ and SI-GaAs antennas with four different values of G at a pump fluence of 70 μJ/cm^2. To control nominal bias field strengths of 3.5 kV/cm for preventing the risk of antenna damage, the bias voltages applied to the anode were 7, 35, 70, and 175 V for $G = 0.02$, 0.1, 0.2, and 0.5 mm, respectively. From Figs. 3a and c, it is seen that each waveform consists of a dominant peak and a minor valley followed by a slowly varying tail. In the time domain, the analysis for these waveforms can be characterized by the absolute value $|E_r^{min}|$ of the THz waveform minimum, the peak and valley full width, and the negative tails. In the frequency domain, we focus on the spectrum bandwidth Δf.

From each waveform, we can clearly identify that the peak width is larger than the valley width, under different values of G. Quantitatively, the value of the peak width is about 0.33 ps less than that reported by Katzenellenbogen

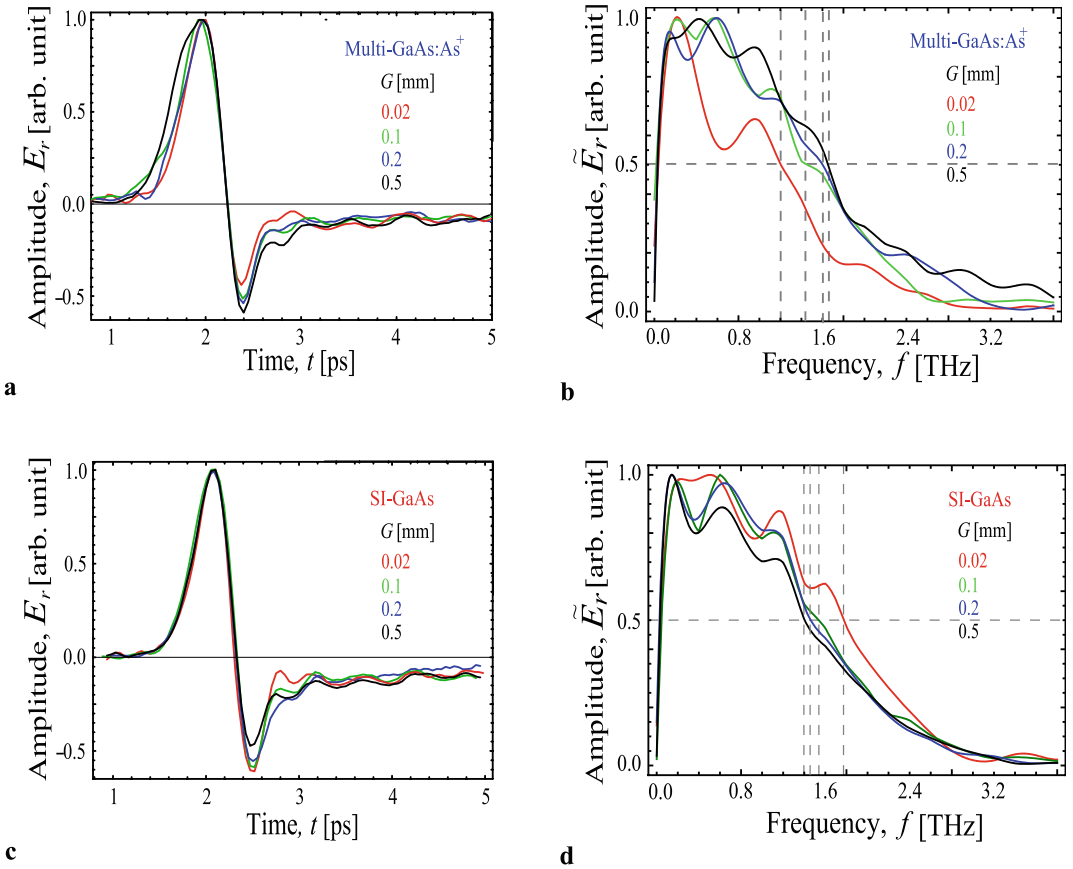

Fig. 3 THz radiation waveforms $E_r(t)$ as a function of time delays t for (**a**) multi-GaAs:As$^+$ and (**c**) SI-GaAs antennas with gap size G of 0.02 (*blue*), 0.1 (*green*), 0.2 (*red*), and 0.5 mm (*black*). (**b**) and (**d**) The corresponding Fourier amplitude $\tilde{E}_r$ spectra

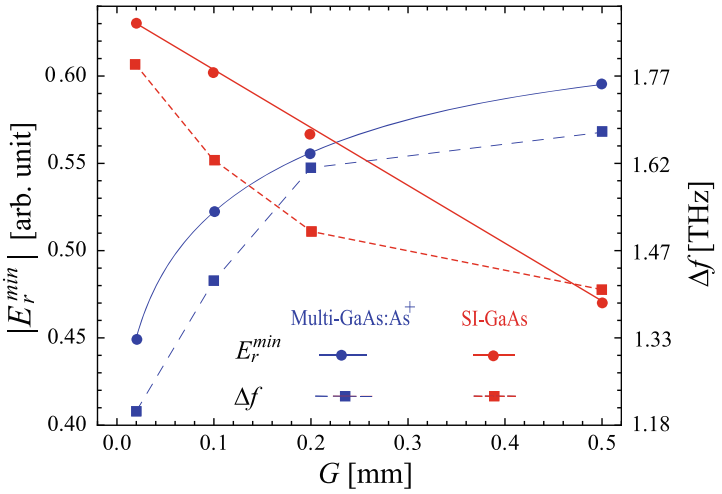

Fig. 4 Bandwidth Δf (*square marks*) and absolute value $|E_{\mathrm{r}}^{\mathrm{min}}|$ (*point marks*) of THz waveform minimum as a function of gap size G for multi-GaAs:As$^+$ (*blue*) and SI-GaAs (*red*) antennas

and Grischkowsky (∼0.38 ps) [20]. Furthermore, for different values of G, the values of the valley width are also different and range irregularly between 0.30 and 0.27 ps without any explicit gap-size dependence. We also observe from each waveform that a relatively long negative tail with the duration of about 3.7 ps follows the valley and is quite obvious in contrast to those found in other similar experiments [8].

From Fig. 3, we obtain the dependences of $|E_{\mathrm{r}}^{\mathrm{min}}|$ and Δf on G and illustrate them in Fig. 4. As can be seen in the case of the multi-GaAs:As$^+$ antenna, as G increases from 0.02 mm to 0.5 mm, Δf increases from 1.2 to 1.6 THz, and $|E_{\mathrm{r}}^{\mathrm{min}}|$ also increases from 0.44 to 0.62 in a strongly nonlinear way, satisfying a saturation function with the form $|E_{\mathrm{r}}^{\mathrm{min}}| = (0.45G^{0.198} + 0.24)/(1 + 0.14G)$, which is also plotted in Fig. 4. On the contrary, in the case of the SI-GaAs antenna, $|E_{\mathrm{r}}^{\mathrm{min}}|$ decreases linearly from 0.64 to 0.47, and Δf also decreases monotonically from 1.77 to 1.41 THz. Obviously, the curves of Δf versus G vary in a manner similar to those of $|E_{\mathrm{r}}^{\mathrm{min}}|$ versus G for both kinds of PC materials. What is especially interesting is that the quantity Δf of multi-GaAs:As$^+$ antennas is smaller for $G = 0.02$ or 0.1 mm, but becomes larger and the spectrum thereby extends to beyond 4.2 THz provided that $G = 0.2$ or 0.5 mm. Accordingly, we infer that under the condition of a large enough gap size the THz radiation from a multi-GaAs:As$^+$ antenna will probably have a larger Δf than that from a SI-GaAs antenna. Indeed, this deduction has been assured to be valid for our previously used large-aperture GaAs:As$^+$ antennas where the numerical simulations confirmed that the larger refractive index and larger absorption coefficient were responsible for the larger Δf [21].

The results of Fig. 4 also point out that the values of Δf are much larger than those produced with a large-aperture SI-GaAs antenna ($\Delta f \sim 0.27$ THz) [5], as well as our previously used small-aperture SI-GaAs or multi-GaAs:As$^+$ antenna ($\Delta f \sim 1$ THz) [12]. This larger Δf is a reflection of a narrow negative peak and a large $|E_{\mathrm{r}}^{\mathrm{min}}|$, and it is just favorable for applications such as THz medical or security imaging requiring broadband THz radiation.

In the introduction, we mentioned that the bias field E_{b}, near the anode of a SI-GaAs or multi-GaAs:As$^+$ antenna is extremely large, so we can make use of this property to acquire a maximum THz power output by focusing a femtosecond laser pulse on that area. For the sake of reaching the same nominal E_{b}, an antenna with a larger G is applied with a higher bias voltage, leading to a higher E_{b} near the anode. As a result, this higher E_{b} significantly increases the space-charge-field screening effect accompanying the larger Δf and $|E_{\mathrm{r}}^{\mathrm{min}}|$ [22]. This explains why Δf and $|E_{\mathrm{r}}^{\mathrm{min}}|$ of a multi-GaAs:As$^+$ antenna increase with the increase of G, but the mechanism leading to the decreasing trend in $|E_{\mathrm{r}}^{\mathrm{min}}|$ of SI-GaAs antennas is unknown to us.

3.2 Bias field and pump fluence dependence

Next, we study how the peak THz amplitude $E_{\mathrm{r}}^{\mathrm{max}}$ varies with the bias field E_{b} and pump fluence F using different PC materials and varying the G factor. Figure 5a plots the E_{b} dependences of $E_{\mathrm{r}}^{\mathrm{max}}$ from SI-GaAs and multi-GaAs:As$^+$ antennas with three different values for G. As seen in this figure, the data reveals linear variations in the case of $G = 0.02$ mm. In the cases of $G = 0.5$ and 1 mm, it is worth noting that nonlinear behaviors occur at both ends of the curves together with linear relationships appearing in the middle parts of the curves. Such nonlinear behaviors become more obvious in the case of multi-GaAs:As$^+$ antennas between 6 and 9 kV/cm, where the amplitude reduction is probably owing to the heating effect within the antennas. This implies that an even higher THz radiation power may be acquired under good cooling apparatus in the pumping area of the sample. Besides, the multi-GaAs:As$^+$ antenna has the advantage of enduring a nominal bias field of as high as

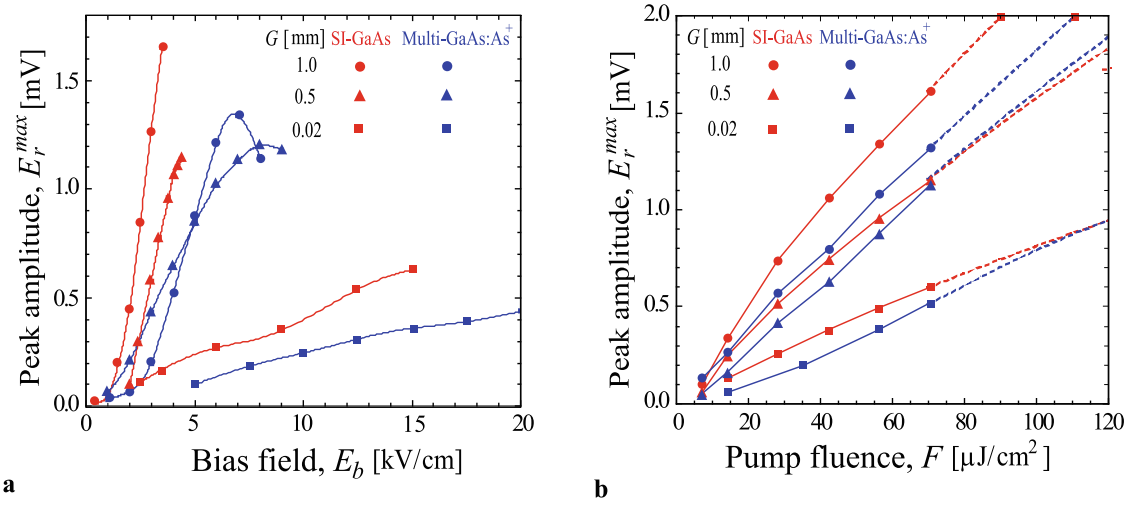

Fig. 5 (**a**) Bias field E_b and (**b**) pump fluence F dependence on peak THz amplitude E_r^{max} for multi-GaAs:As$^+$ (*blue*) and SI-GaAs (*red*) antennas with gap size G of 0.02 (*square marks*), 0.5 (*triangle marks*), and 1 mm (*point marks*). The pump fluence F is fixed at 70 μJ/cm^2 in (**a**), and the nominal bias field E_b is kept at 3.5 kV/cm in (**b**)

8 kV/cm without causing any electrical damage to itself under photoexcitation. By contrast, the bias field applied to the SI-GaAs antenna has to be constrained below the threshold of 4 kV/cm to prevent electrical damage to the device.

The F dependences of E_r^{max} are plotted in Fig. 5b where E_r^{max} increases monotonically with the increase of F for each material and G. We also found that the antenna with a larger G possesses a higher E_r^{max} for each material, and E_r^{max} of a multi-GaAs:As$^+$ antenna is lower than that of a SI-GaAs antenna in the measurable range (i.e. 0–70 μJ/cm^2) with the same G. Nevertheless, we perceive that E_r^{max} from SI-GaAs antennas reveals slightly saturated trends at a high F, leading to a reverse consequence that if F is over 70 μJ/cm^2 E_r^{max} from multi-GaAs:As$^+$ antennas will be expected to be higher than the SI-GaAs cases, according to the experimental data using the scaling rule [17].

In the following, we employ the scaling rule to interpret the observations in Fig. 5. It is known that the scaling rule relates E_r^{max} to both E_b and F by the formula

$$E_r^{max} \approx D\frac{F}{F_s + F}, \tag{1}$$

where

$$D = \frac{A\sqrt{n_L}E_b}{4\pi\varepsilon_0 c^2 \eta_0 \tau_d z}, \tag{2}$$

$$F_s = \frac{(1+n_L)h\nu}{q(1-R)\mu_e\eta_0}. \tag{3}$$

In this notation, n_L is the refractive index, μ_e is the electron mobility, A refers to the pump spot area, and $h\nu$ is the photon energy.

As described in the aforementioned experimental conditions, the diameter of our pump spot area stays at about 0.1 mm, corresponding to an area of 7.8×10^{-3} mm^2. For the cases of $G = 0.02$, 0.5, and 1 mm, the values of A are equal to the gap area 3.1×10^{-4} mm^2 in the former case, but equal to the pump spot size 7.8×10^{-3} mm^2 in the latter two cases as indicated in Fig. 1. According to (1) and (2), E_r^{max} of a 0.02-mm-gap antenna is proportional to A, and thus has a lower value either in the bias or pump fluence dependence since its value of A is smaller than the other two cases. As a matter of fact, although the latter two cases have the same value of A, the value of E_r^{max} of a 1-mm-gap antenna is higher than that of a 0.5-mm-gap antenna rather than having the same value of E_r^{max}. The reason is because the strength of the trap-enhanced bias field E_b near the anode depends on G. As we have mentioned in subsection A, if one applies the same nominal bias field to each antenna, the larger G, the higher E_b near the anode. Thus, E_r^{max} of a 1-mm-gap antenna with a higher E_b is higher than that of a 0.5-mm-gap antenna with a lower E_b according to (2).

In (1) and (2), n_L and μ_e show involvement with the optical and electrical properties of PC materials. Due to ion implantation, the values of n_L for a multi-GaAs:As$^+$ antenna are larger than those of a SI-GaAs antenna, and the effective μ_e of a multi-GaAs:As$^+$ antenna is estimated to be about 1500 cm^2/V s less than that of a SI-GaAs antenna ($\mu_e \sim 5000$ cm^2/V s). According to (3), a larger n_L and a smaller μ_e correspond to larger D and F_s, leading to E_r^{max} of a multi-GaAs:As$^+$ antenna being lower than a specific F but becoming higher than a specific F at the same G. For $G = 0.5$ mm, the fit to the experimental data of Fig. 5b yields $D = 15.6$, $F_s = 870.5$ μJ/cm^2 for a multi-GaAs:As$^+$ antenna and $D = 10.2$, $F_s = 550.5$ μJ/cm^2 for a SI-GaAs antenna. According to these two fits, it can be seen that E_r^{max} of a 0.5-mm-gap multi-GaAs:As$^+$ antenna is lower than that

of a SI-GaAs antenna if $F < 70\ \mu J/cm^2$, but becomes higher if $F > 70\ \mu J/cm^2$. Similar phenomena have also been found in our large-aperture GaAs:As^+ antennas [21], and hence we believe that the mid-aperture multi-GaAs:As^+ antennas will benefit from high pump fluence as well.

4 Conclusions

We have presented a study of gap-size-dependent phenomena on THz radiation. We used several multi-GaAs:As^+ and SI-GaAs mid-aperture antennas with different bias voltages and gap sizes to observe their bipolar THz waveforms in an optical pump–probe experiment. At fixed pump fluence and nominal bias field, with the increase of gap size of the antennas, we observe that both the bandwidth of the THz radiation and the absolute value of the THz waveform minimum decrease linearly for SI-GaAs antennas, whereas they increase monotonically for multi-GaAs:As^+ antennas, resulting in a consequence that the bandwidth from a multi-GaAs:As^+ antenna is larger than that from a SI-GaAs antenna at a large gap size. The bandwidths of the THz radiations from our antennas are considerably larger compared to other small- or large-aperture antennas. In the dependences of bias field and pump fluence on the peak THz amplitude, the measured data and associated theoretical prediction curves indicate that the multi-GaAs:As^+ antenna benefits from its higher reachable bias fields, and can generate even higher THz power, probably at high pump fluence, in comparison with a SI-GaAs antenna.

Acknowledgements This work was partially supported by the Academic Top Universities Program of the Ministry of Education and various grants of the National Science Council of Taiwan, Republic of China.

References

1. H.M. Pickett, J. Mol. Spectrosc. **148**, 371 (1991)
2. T.R. Globus, D.L. Woolard, T. Khromova, T.W. Crowe, M. Bykhovskaia, B.L. Gelmont, Hesler, A.C. Samuels, J. Biol. Phys. **29**, 89 (2003)
3. D.M. Mittleman, M. Gupta, R. Neelamani, R. Baraniuk, J.V. Rudd, M. Koch, Appl. Phys. B: Photophys. Laser Chem. **68**, 1085 (1999)
4. T.-A. Liu, G.-R. Lin, Y.-C. Chang, C.-L. Pan, Opt. Express **13**, 10416 (2005)
5. T. Hattori, K. Tukamoto, H. Nakatsuka, Jpn. J. Appl. Phys. **40**, 4907 (2001)
6. M.S. Markram-Ebied, in *Semi-insulating III–V Materials*, ed. by D.C. Look, J.S. Blakemore (Shiva, Nantwich, 1984)
7. F.W. Smith, H.Q. Le, V. Diaduk, M.A. Hollis, A.R. Calawa, S. Gupta, M. Frankel, D.R. Dykaar, G.A. Mourou, T.Y. Hsiang, Appl. Phys. Lett. **54**, 890 (1989)
8. M. Tani, S. Matsuura, K. Sakai, S. Nakashima, Appl. Opt. **36**, 7853 (1997)
9. K.G. Eyink, M.A. Capano, S.D. Walck, T.W. Haas, B.G. Streetman, J. Electron. Mater. **26**, 391 (1997)
10. A. Hussain, S.R. Andrews, Appl. Phys. Lett. **88**, 143514 (2006)
11. J. Lloyd-Hughes, E. Castro-Camus, M.D. Fraser, C. Jagadish, M.B. Johnston, Phys. Rev. B **70**, 235330 (2004)
12. T.-A. Liu, M. Tani, C.-L. Pan, J. Appl. Phys. **93**, 2996 (2003)
13. T.-A. Liu, G.-R. Lin, Y.-C. Lee, S.-C. Wang, M. Tani, H.-H. Wu, C.-L. Pan, J. Appl. Phys. **98**, 013711 (2005)
14. J.T. Darrow, X.-C. Zhang, D.H. Auston, Appl. Phys. Lett. **58**, 25 (1990)
15. J.T. Darrow, X.-C. Zhang, D.H. Auston, J.D. Morse, IEEE J. Quantum Electron. **28**, 1607 (1992)
16. P.K. Benicewicz, A.J. Taylor, Opt. Lett. **18**, 1332 (1993)
17. P.K. Benicewicz, J.P. Roberts, A.J. Taylor, J. Opt. Soc. Am. B **11**, 2533 (1994)
18. S.E. Ralph, D. Grischkowsky, Appl. Phys. Lett. **59**, 1972 (1991)
19. Q. Wu, X.-C. Zhang, Appl. Phys. Lett. **67**, 3523 (1995)
20. N. Katzenellenbogen, D. Grischkowsky, Appl. Phys. Lett. **58**, 222 (1991)
21. R.-H. Chou, T.-A. Liu, C.-L. Pan, J. Appl. Phys. **104**, 053121 (2008)
22. R.-H. Chou, T.-A. Liu, C.-L. Pan, Jpn. J. Appl. Phys. **47**, 8419 (2008)